# Coordination Arrays: Synthesis and Characterisation of Rack-Type Dinuclear Complexes

**Garry S. Hanan, Claudia R. Arana, Jean-Marie Lehn,* Gerhard Baum and Dieter Fenske**

**Abstract**: A series of mono- and dimetallic complexes of rack type containing a dinucleating bis-tridentate ligand and $Ru^{II}$–2,2′:6′,2″-terpyridyl (tpy) sites were synthesised and characterised. The $^1H$ NMR spectra of the dimetallic complexes were correlated to structural features, and the crystal structures of the dimetallic complexes were determined. They provide information about the way in which the central substituent affects the overall shape of the racks and the relative disposition of the metal centres, measured by the pinching angle of the bis-tridentate ligand and the convergence angle of the ancillary tpy units. The latter demonstrates that a $CH_3$ group yields the least bent complex and indicates how parallel the tpy units are. The dimetallic racks exhibit metal–metal interactions mediated by the bis-tridentate ligands as indicated by electrochemical and spectroscopic methods. The bridging-ligand $\pi^*$ orbital and the $d_\pi$ metal orbital are stabilised by complexation of a second metal. The results obtained provide guidelines for the design of extended racks bearing several metal centres in a linear arrangement, which also represent potential components of molecular electronic devices.

**Keywords**
complexes with nitrogen ligands · ruthenium complexes · self-assembly · supramolecular chemistry

## Introduction

The synthesis of coordination arrays, supramolecular-level structures of precise nuclearity and defined geometry, is one of our current research interests.[1–3] These species are ordered inorganic architectures comprising one- or two-dimensional geometries of $[m \times n]$ nuclearity and presenting in sequence of increasing complexity basic geometries that may be termed *racks* $[n]$R, *ladders* $[2n]$L and *grids* $[m \times n]$G (Fig. 1), where the nuclearity of the R, L and G species is given by $[n]$, $[2n]$ and $[m \times n]$, with $n$ (for a square grid) representing their rank. More complex structures involving extension into three dimensions and long-range lattices may be envisaged.

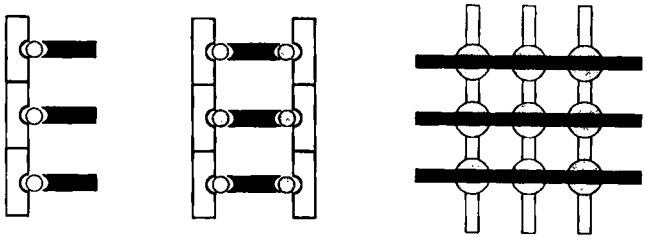

Fig. 1. Schematic representation of polymetallic coordination arrays: racks (left), ladders (centre) and grids (right).

The assembly of such inorganic arrays requires the choice of a suitable binding subunit–metal ion combination leading to a perpendicular disposition of the ligands through metal ion coordination at their crossing points. This can be achieved with planar ligand subunits of either bidentate or tridentate type connected through metal ions of tetrahedral or octahedral coordination geometry, respectively (Fig. 2). In addition to serving as centres for ligand binding and positioning, the metal ions also introduce specific electrochemical, photochemical and reaction properties, thus conferring functionality to the final architectures for development towards inorganic supramolecular devices.[4, 5]

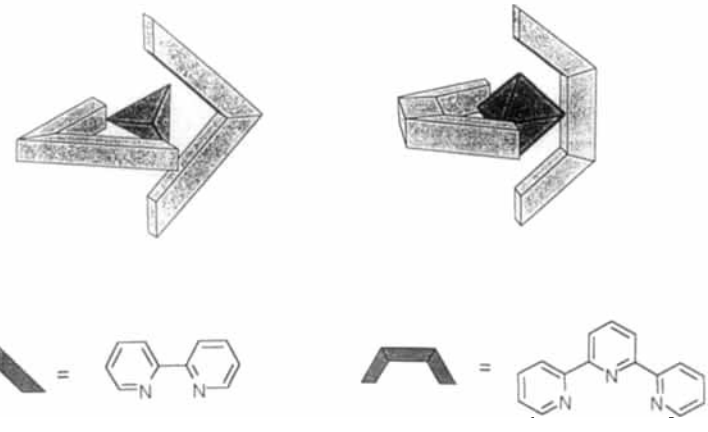

Fig. 2. Building blocks for perpendicular coordination arrangements: bipyridine or terpyridine units and tetrahedral or octahedral coordination, respectively.

[*] Prof. Dr. J.-M. Lehn, G. S. Hanan, Dr. C. Arana
Laboratoire de Chimie Supramoléculaire, Institut Le Bel,
Université Louis Pasteur
4, rue Blaise Pascal, F-67000 Strasbourg (France)
Fax: Int. code +(88)41-1020
Prof. Dr. D. Fenske, G. Baum
Institut für Anorganische Chemie der Universität
Engesserstrasse, D-76128 Karlsruhe (Germany)



0947-6539/96/0210-1292 $ 15.00+.25/0

The thermodynamic and kinetic stability of such species in the ground and excited states depends on the choice of metal ion and ligand. Stable complexes are formed by chelating binding units,[6] such as 2,2′-bipyridine (bpy)[7] and 2,2′:6′,2″-terpyridine (tpy),[8] which can withstand a variety of oxidative and reductive conditions. They are good σ and π donors and π acceptors, and are thus capable of stabilising both high and low oxidation states of metal ions.[7, 8] Bpy and tpy are well-suited as binding subunits in coordination arrays, since their complexes exhibit the required structural features as well as accessible π* orbitals and photostability.[9]

The self-assembly of polynuclear ion grids from rigid ligands containing bidentate sites and $Ag^{I}$[3] or $Cu^{I}$[10] ions has been reported earlier. Metal ions with octahedral coordination geometry are much more abundant and their complexes usually present a much richer palette of physical and chemical properties than the tetrahedrally coordinated $Ag^{I}$ and $Cu^{I}$ ions. We thus undertook to design and study polynuclear coordination arrays based on tridentate subunits and octahedral metal ions.

Herein we describe the synthesis of the dinuclear rigid rack complexes **2a–d** and of their mononuclear analogues **1a–c** based on the ligands **3a–d**, containing two sites of tpy type and

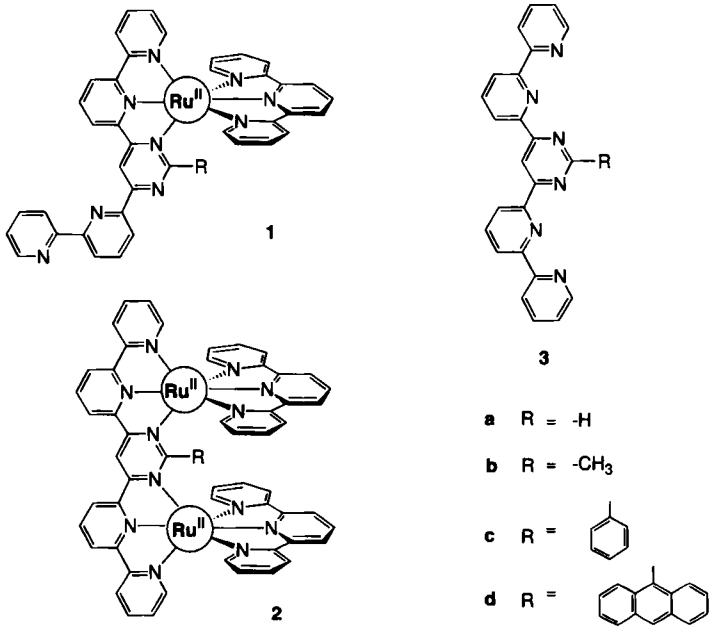


two or one $Ru(tpy)^{2+}$ centres, as well as the crystal structures and electrochemical properties of these complexes. Trinuclear species[11] and grid-type[12] arrays based on similar components will be reported later. A variety of octahedral metal ions have been used to assemble metallosupramolecular structures[13] and the coordination arrays formed depend on the choice of ligand. Compounds **3** represent a ligand system that fulfills the present purposes and incorporates a known metal–metal electronic mediator, pyrimidine.[14]

**Abstract in French**: *Des complexes bimétalliques composés de ruthénium, 2,2′:6′,2″-terpyridine et des ligands bis-tridentates ont été synthétisés et caractérisés. Les interactions métaux–métaux ont été mesurées par des méthodes spectroscopiques et électrochimiques. L'extension à des systèmes polymétalliques est discutée.*

## Results and Discussion

**Synthesis of the rack complexes**: The reaction of 2.5 equivalents of $Ru(tpy)Cl_3$ with the bis-tridentate ligands **3a–d** in protic solvents, or mixtures of water and another protic solvent, gave deep green mixtures. Addition of aqueous ammonium hexafluorophosphate ($[NH_4][PF_6]$) led to the precipitation of green solids, which were purified by successive recrystallisation from acetonitrile/toluene or by column chromatography on alumina with acetonitrile/toluene mixtures as eluant to give the dimetallic complexes **2a–d**. The solvent also functioned as electron donor for the $Ru^{III}$–$Ru^{II}$ conversion. To synthesise **2d**, *N*-ethylmorpholine was required for the reaction to proceed in good yields.

The monometallic complexes **1a–d** were produced as byproducts in the synthesis of the dimetallic ones and were not easily obtained as the primary product. Regardless of the number of equivalents of ligand or $Ru(tpy)Cl_3$ used, the most abundant product was the dimetallic species. Dinuclear complexes are said to form because of "charge-transfer-associated polynucleation",[15–17] where the coordination of a first back-donating metal fragment increases the basicity of the remaining donor atoms so as to enhance a second coordination.[16] Consequently, another $[Ru(tpy)]^{2+}$ moiety may react preferentially with a monometallic complex to form a dimetallic one rather than with a free ligand to form a monometallic complex.

**Crystal structures of mononuclear and dinuclear rack complexes**: The crystal structures of the rack complexes **1c** and **2a–d** are represented in Figures 3–7; selected bond angles, bond lengths and characteristic structural features are given in Tables 1–4.

$[\{Ru(tpy)\}_2(\mathbf{3a})][PF_6]_4$ (**2a**) crystallises with four molecules per unit cell. Each molecule has a mirror plane through the C2–C5 axis of the central pyrimidine (Fig. 3). The X-ray structure of **2a** verifies that **3a** acts as a bis-tridentate ligand coordinating two Ru atoms by two sets of *mer*-$N_3$ donors, with the other three coordination sites of each Ru atom occupied by a *mer*-tridentate tpy. The Ru atoms are in identical, pseudooctahedral environments.

The N1-Ru-N7 and N1-Ru-N9 angles (86.2(2)° and 95.9(2)°, respectively) are almost complementary to the N3-Ru-N7 and N3-Ru-N9 angles (98.6(2)° and 88.1(2)°, respectively) (Fig. 3a, Table 1). The combination of acute and obtuse angles draws two terminal pyridines together (centroid-to-centroid distance ctc = 4.670 Å) and separates the two others (ctc = 7.629 Å). The central pyridines of the tpy's are even closer together, with ctc = 4.414 Å. The angle (40.7°) and the distance (C4–C4′ = 3.51 Å) between these heterocyclic rings are an indication of π-stacking interactions between them, perhaps at the origin of the dissymmetry of each individual tpy in the solid state.

An acetone molecule is located between the converging ancillary tpy's; each methyl group of the acetone molecule is directed towards one of their terminal pyridines (Fig. 3b). The closest contact distance is to C4 of the ring incorporating N7, at 3.703 Å. The planes of the two terminal pyridines make a dihedral angle of 22.5° with the plane of the central pyridine of the tpy's.

$[\{Ru(tpy)\}_2(\mathbf{3b})][PF_6]_4$ (**2b**) crystallises with two molecules per unit cell. Its X-ray structure (Fig. 4) confirms that **3b** acts as a bis-tridentate ligand coordinating two Ru atoms in the same way as in **2a**. The Ru atoms are in nonequivalent, pseudooctahedral environments bonded to three N atoms of **3b** and three N atoms of tpy. The N-Ru-N five-membered chelate ring angles are similar to those found in **2a** (Table 1). The N2-Ru-N8 angle

  0947-6539/96/0210-1293 $ 15.00+.25/0 

Table 1. Averaged N-Ru-N angles (°) from the X-ray structures of complexes **1c**, **2a**–**d** [a].

| Complex | N7-Ru-N8<br>N1-Ru-N2 | N8-Ru-N9<br>N2-Ru-N3 | N7-Ru-N9 (/2)<br>N1-Ru-N3 (/2) | N2-Ru-N8 | N1-Ru-N7<br>N1-Ru-N9 | N3-Ru-N7<br>N3-Ru-N9 |
|---|---|---|---|---|---|---|
| **1c** | 78.7 | 79.1 | 157.8 (78.6) | 174.8 | 87.7 | 97.9 |
| | 79.4 | 77.7 | 157.1 (78.9) | | 96.1 | 87.1 |
| **2a** | 78.7 | 79.1 | 157.6 (78.8) | 178.5 | 86.2 | 98.6 |
| | 78.5 | 79.0 | 157.5 (78.8) | | 95.9 | 88.1 |
| **2b** | 79.3±0.4 | 78±1 | 157±2 (78.5) | 172±2 | 91.6±0.5 | 93.4±0.2 |
| | 79.2±0.4 | 77.9±0.8 | 157±1 (78.5) | | 94.0±0.9 | 90.0±0.9 |
| **2c** | 79.3±0.2 | 79±1 | 157±2 (78.8) | 172±2 | 93.0±0.3 | 92.7±0 |
| | 79.0±0.4 | 78.2±0.6 | 157±1 (78.8) | | 93±2 | 90.2±0.3 |
| **2d** | 78.8±0.5 | 79.1±0.2 | 158±1 (79) | 171.8±0.9 | 90±2 | 93.2±0 |
| | 79.2±0.6 | 78.0±0.5 | 157.2±0.7 (78.4) | | 91±1 | 94.0±0.5 |

[a] Values are averaged for the two tridentate sites in **2b**–**d** (e.g., in column 1, N7-Ru-N8 = (N7-Ru1-N8 + N10-Ru2-N11)/2).

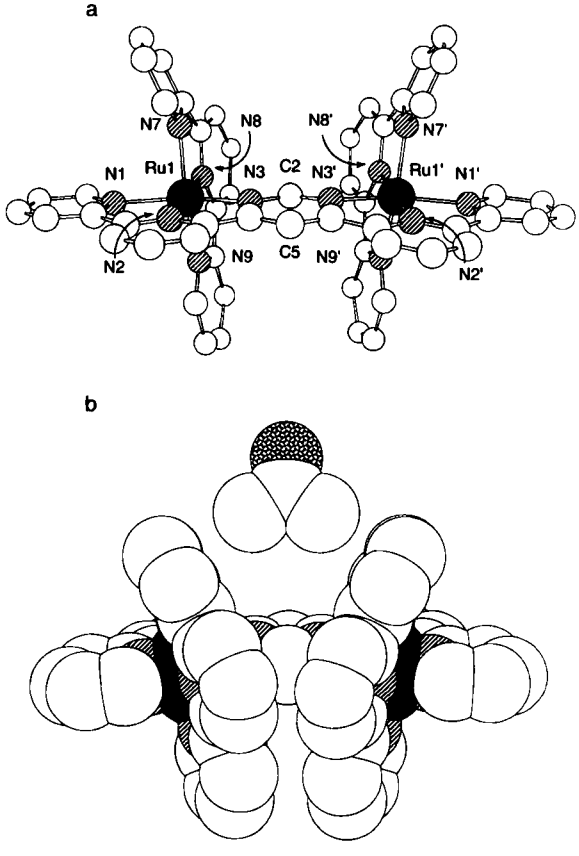


Fig. 3. a) Ball and stick and b) space-filling representations of the crystal structure of bimetallic complex **2a** (the orientations of the two representations differ by 180°; the acetone molecule of crystallisation has been omitted in a).

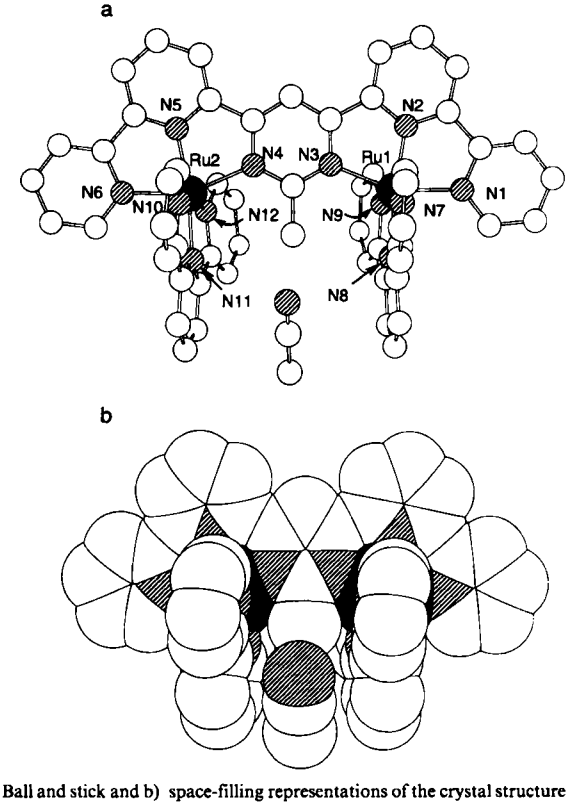


Fig. 4. a) Ball and stick and b) space-filling representations of the crystal structure of bimetallic complex **2b**.

is 172±2°, with a difference of 2.4° between the two angles. The angles N1-Ru-N7, N1-Ru-N9, N3-Ru-N7 and N3-Ru-N9 are closer to 90° than in **2a**. However, two terminal pyridines are close together and two others are apart (ctc = 4.524 and 7.009 Å, respectively, Fig. 4a). The ctc distance between the central pyridines of the tpy's is 6.210 Å, indicating that the tpy's do not converge as in **2a**. This may be attributed to the steric effect of the insertion of a $CH_3$ group between these two py's, as indicated by the distortion of ligand **3b**.

An acetonitrile molecule is perched above the two separated terminal pyridines in **2b**, with the methyl group pointed towards the narrower part of the separation (Fig. 4b). The acetonitrile methyl-carbon-to-pyridine C4 distance (3.588 Å) may indicate Van der Waals and/or weak CH–π interaction.[18, 19] Also, the N atom of the acetonitrile is approx. 3.4 Å from the methyl group of **3b**, suggesting CH–N interaction.

[{Ru(tpy)}$_2$(**3c**)][$PF_6$]$_4$ (**2c**): The bis-tridentate ligand **3c** coordinates two Ru atoms in an analogous fashion to **3b** in **2b** (Fig. 5a). The Ru atoms are in crystallographically nonequivalent, pseudooctahedral environments with Ru–pyridine N bond lengths similar to those in **2a** and **2b**, but with slightly greater Ru–pyrimidine bond lengths (2.13±0.01 Å) (Table 2). The N-Ru-N bond angles are similar to those in the two previous structures. The N1-Ru-N3 (157±1°) and N7-Ru-N9 (157±2°) angles are slightly larger than those of **2b**, but similar to that of $[Ru(tpy)_2]^{2+}$ (≈157°).[20, 21] The angles N2-Ru1-N8 and N5-Ru2-N11 are averaged at 172±2°, with a difference of 2.0° between the two angles.

The angles between N atoms from different tridentate sites are similar to those in **2b**. The two terminal pyridines are drawn together in **2c** (ctc = 5.257 Å), but not to the same extent as in **2a** and **2b**. The ctc distance between the central pyridines of the

  0947-6539/96/0210-1294 $ 15.00+.25/0 Chem. Eur. J. 1996, 2, No. 10

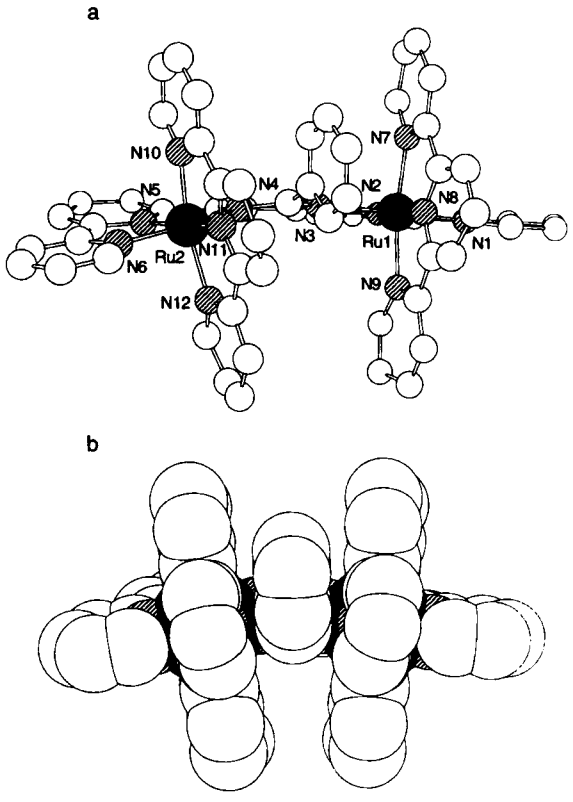


Fig. 5. a) Ball and stick and b) space-filling representation of the crystal structure of bimetallic complex **2c**.

Table 2. Ru–N bond lengths and Ru–Ru distances (Å) from the X-ray structures of complexes **1c** and **2a–d** [a].

| | Ru1–N1<br>Ru2–N6 | Ru1–N2<br>Ru2–N5 | Ru1–N3<br>Ru2–N4 | Ru1–N7<br>Ru2–N10 | Ru1–N8<br>Ru2–N11 | Ru1–N9<br>Ru2–N12 | Ru–Ru |
|---|---|---|---|---|---|---|---|
| **1c** | 2.065(5) | 1.979(5) | 2.121(4) | 2.066(5) | 1.986(5) | 2.074(5) | – |
| **2a** [a] | 2.090(5) | 1.988(5) | 2.084(4) | 2.090(5) | 1.993(5) | 2.092(5) | 6.160 |
| **2b** | 2.060(5) | 1.996(5) | 2.128(5) | 2.074(5) | 2.000(5) | 2.067(6) | 6.263 |
| | 2.054(5) | 2.008(5) | 2.135(5) | 2.095(5) | 2.010(5) | 2.117(6) | |
| **2c** | 2.063(5) | 1.976(5) | 2.127(5) | 2.072(5) | 1.965(5) | 2.069(5) | 6.273 |
| | 2.079(5) | 1.983(5) | 2.139(5) | 2.074(5) | 1.975(5) | 2.100(5) | |
| **2d** | 2.065(4) | 1.980(5) | 2.148(4) | 2.078(5) | 1.993(5) | 2.076(5) | 6.405 |
| | 2.067(4) | 2.001(5) | 2.151(4) | 2.073(5) | 2.000(5) | 2.080(5) | |

[a] Symmetric about the pyrimidine C2–C5 axis.

tpy's is 6.230 Å. No solvent molecules are in close contact with the complex; this may be an indication that less space is available between the two tpy's because of the pyrimidine C2 phenyl substituent. The centre of the phenyl group lies above the average plane of the bis-tridentate ligand **3c**, minimising the steric compression with the tpy's (Fig. 5b) while retaining $\pi$-stacking.[22]

In $[\{Ru(tpy)\}_2(\mathbf{3d})][PF_6]_4$ (**2d**), two Ru atoms coordinate to each *mer*-tridentate site in **3d**, with the other Ru coordination sites occupied by *mer*-tpy's (Fig. 6). The Ru atoms are crystallographically nonequivalent and are in pseudooctahedral coordination environments. The averaged Ru–pyrimidine-N bond length is the longest of the dimetallic complexes (2.150 ± 0.003 Å), whereas the averaged Ru–pyridine-N bond lengths are similar to those of the other dimetallic complexes. The N-Ru-N angles in the five-membered chelate rings are within ±0.2° of the angles in **2c**. The N1-Ru-N3 and N7-Ru-N9 angles are 157.2 ± 0.7° and 158 ± 1°, respectively, the largest values for these angles found in the dimetallic complexes. The

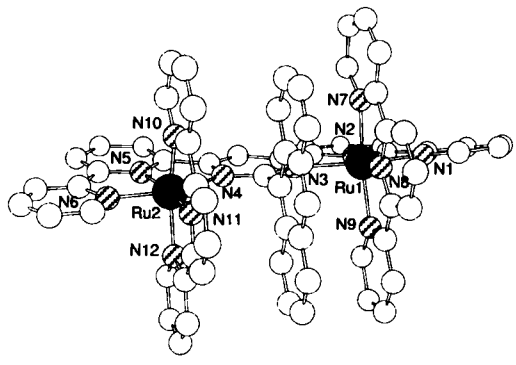


Fig. 6. Ball and stick representation of the crystal structure of bimetallic complex **2d**.

N2-Ru-N8 (171.8 ± 0.9°) and N5-Ru-N11 (171.3(2)°) angles are the farthest from linearity of the dimetallic complexes.

The other N-Ru-N bond angles are similar to those in **2c**. The terminal pyridines are separated by almost the same distance (ctc = 6.454 and 6.526 Å for rings 7–10 and 9–12, respectively; ring numbers are the same as those of N atoms), creating no discernible openings between the tpy's for solvent interactions. The distance between the central pyridines of the tpy's (ctc = 6.778 Å) is longer than in **2c**, owing to compression with the 9-anthryl moiety, which is almost perpendicular to the heterocyclic portion of **3d** (Fig. 6).

$[Ru(tpy)(\mathbf{3c})][PF_6]_2$ (**1c**) crystallises with four molecules in the asymmetric unit. One tridentate site of **3c** is coordinated to a Ru atom and the other is unoccupied (Fig. 7a). The pseudooctahedral coordination environment of the Ru atom is completed by a *mer*-$N_3$ tpy donor. The Ru–N bond lengths are less than 1% different from those in **2c**. The uncoordinated N atoms are *trans*

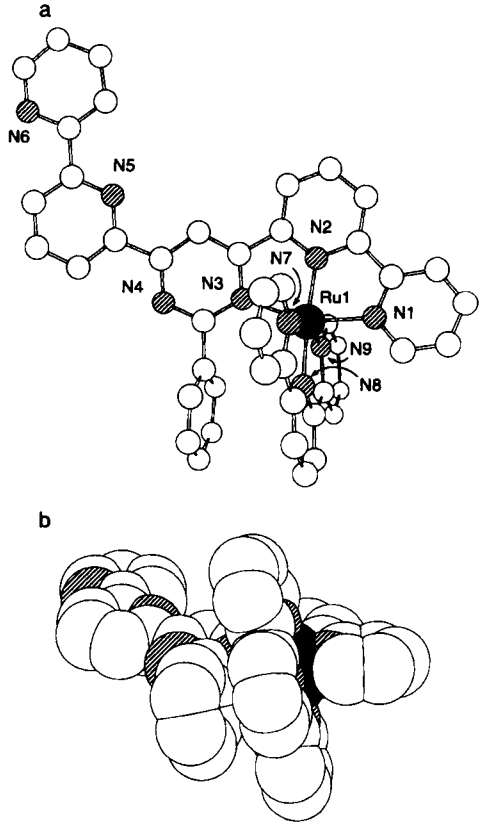


Fig. 7. a) Ball and stick and b) space-filling representation of the crystal structure of bimetallic complex **1c**.

about the interannular bonds to the adjacent heterocycles, leaving the uncoordinated bipyridyl moiety away from the pyrimidine C2 position. The five-membered chelate rings have N1-Ru-N2 (79.4(2)°), N2-Ru-N3 (77.7(2)°), N7-Ru-N8 (78.7(2)°) and N8-Ru-N9 (79.1(2)°) angles resembling those of the dimetallic complex **2a**, as do the N1-Ru-N3 and N7-Ru-N9 angles (157.1(2)° and 157.8(2)°, respectively) and the N2-Ru-N8 angle (174.8(2)°). The planes formed by the five-membered chelate rings have dihedral angles ranging from 80.8(2)° to 83.0(3)° and are clearly not perpendicular to one another. There are notable deviations from 90° for the angles between terminal N's from different tridentate sites. The tpy is, therefore, not perpendicular to the backbone of **3c**, although it is parallel to its phenyl group (Fig. 7b). The phenyl group in **3c** and the tpy are in Van der Waals contact (ctc = 3.450 Å). The phenyl group is distorted off-centre from the central pyridine of the tpy. No significant intermolecular contacts with solvent molecules are observed in the solid state.

The comparative structural changes along the series **2a–d** show how the central substituent influences characteristic geometrical features of the dinuclear rack complexes.

Thus, the metal-to-metal distances Ru–Ru increase along the series **2a–d** from 6.160 to 6.405 Å (Table 2) along with the size of the substituent.

Pinching angles and convergence angles (Fig. 8, Table 3) provide information about the shape of the complexes. The order of decreasing pinching angle (Fig. 8a) is related to the size of the pyrimidine C2 substituent: R = hydrogen > phenyl > methyl > 9-anthryl. The difference between R = phenyl and R = methyl is not significant; however, the 9-anthryl group has a smaller pinching angle, which may reflect the extended contact between the 9-anthryl group and the tpy's.

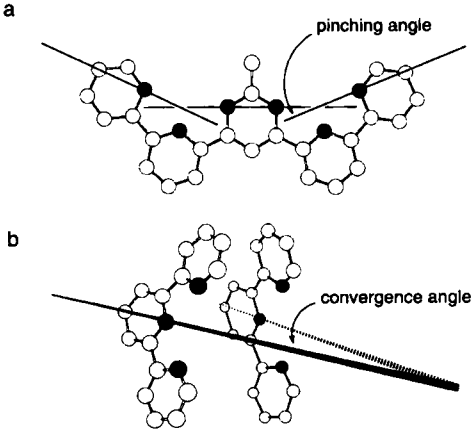


Fig. 8. a) Pinching and b) convergence angles in the crystal structure of the bimetallic complexes **2**.

Table 3. Pinching and convergence angles from the X-ray structures.

| | **2a** | **2b** | **2c** | **2d** |
|---|---|---|---|---|
| C4–C4 (Å) | 3.508 | 6.386 | 6.465 | 7.173 |
| N8–N11 (Å) | 5.181 | 6.056 | 6.076 | 6.382 |
| Convergence angle (°) | 36.3 | 7.2 | 9.5 | 21.8 |
| Pinching angle (°) | 25.6 | 24.0 | 25.4 | 21.8 |

The angle between the vectors drawn through the N atom and C4 of the central pyridine of each tpy, defined as the convergence angle (Fig. 8b), provides an indication of the effect of the central R group on the parallelism of the ancillary tpy's and thus on the linearity (or bending) of a rack ligand **3** in the rack complexes **2** as a function of the nature of R. The ctc distance of the central py's of the ancillary tpy's increases markedly along the series: **2a**, 4.414 Å; **2b**, 6.210 Å; **2c**, 6.230 Å and **2d**, 6.778 Å.

As the X-ray structures of the dimetallic complexes illustrate, **2a** has convergent ancillary tpy's. The tpy's in the other dimetallic complexes are divergent. By the convergence angle criterion, the methyl-substituted complex **2b**, which is the least bent, appears to be best suited for assembling larger racks, ladders and grids.

The values for the C–C and C–N bond lengths are compiled in Table 4, with the values for free tridentate sites given in parentheses. The py–py interannular bond lengths decrease and the py–CN bond lengths increase, as previously noted for metal–terpy complexes.[23] The py–pym interannular bond lengths are shorter than the py–py ones; this was also found for a related ligand.[24] The pyrimidine C–N bond lengths increase upon coordination and vary somewhat among the dimetallic complexes.

Direct comparison of coordinated and uncoordinated tridentate sites is possible for the monometallic complex **1c**. The tpy and the bpy moiety of the coordinated tridentate sites exhibit similar shortening of the C–C bond upon complexation compared with tpy. However, the bpy moiety in the free tridentate site remains relatively unchanged. The pym–py C–C bond length is notably longer (Δ = 0.27 Å) in the free tridentate site than in the coordinated one. The C–N bond lengths of the coordinated pyridines and pyrimidines increase upon metal complexation, although they remain relatively unchanged in the free tridentate site as compared with tpy.

Table 4. Inter-heterocyclic C–C bond lengths (Å) and angles (°) from the X-ray structures [a].

| | Ligand | C–C py (free) | C–C pym–py (free) | C–N py (free) | C–N pym (free) | C-N-C py (free) | C-N-C pym (free) | C-C-N py (free) | C-C-N pym (free) |
|---|---|---|---|---|---|---|---|---|---|
| | tpy | (1.490) | – | (1.342) | | (117.5) | | (117.0) | |
| **1c** | tpy | 1.470 | | 1.352 | | 121.2 | | 112.4 | |
| | **3c** | 1.460 | 1.463 | 1.359 | 1.367 | 121.3 | 116.1 | 112.9 | 115.3 |
| | | (1.495) | (1.490) | (1.342) | (1.338) | (117.6) | (118.2) | (116.6) | (116.1) |
| **2a** | tpy | 1.466 | | 1.355 | | 122.3 | | 113.0 | |
| | **3a** | 1.469 | 1.469 | 1.354 | 1.352 | 121.5 | 118.7 | 112.5 | 116.2 |
| **2b** | tpy | 1.480 | | 1.353 | | 122.5 | | 113.1 | |
| | **3b** | 1.462 | 1.456 | 1.357 | 1.358 | 121.4 | 118.2 | 112.9 | 116.5 |
| **2c** | tpy | 1.473 | | 1.357 | | 121.1 | | 112.4 | |
| | **3c** | 1.473 | 1.465 | 1.359 | 1.360 | 120.3 | 117.2 | 112.3 | 116.2 |
| **2d** | tpy | 1.471 | | 1.352 | | 121.8 | | 112.9 | |
| | **3d** | | 1.466 | 1.355 | 1.365 | 120.7 | 116.9 | 112.6 | 116.7 |

[a] Values for the uncoordinated sites given in parentheses.



0947-6539/96/0210-1296 $ 15.00+.25/0 Chem. Eur. J. 1996, 2, No. 10

The principal angular distortion in tpy upon metal complexation is the increase in the central pyridine C-N-C angle and the decrease in the inter-pyridine C-C-N angle.[23] The dimetallic complexes exhibit this feature as well, in the tpy's and in the bipyridyl moieties of the bis-tridentate ligands. The C-N-C and C-C-N angles involving the N atoms from the central pyrimidine exhibit identical trends (C-N-C increase and C-C-N decrease) when compared with the C-N-C and C-C-N angles for a related ligand.[24] The C-N-C and C-C-N angles for pyrimidine are smaller and greater, respectively, than for pyridine. In **1c**, the C-N-C and C-C-N angles are relatively unchanged for the free tridentate site as compared with tpy,[23] whereas the bound tridentate site shows similar changes as for the dimetallic complexes. The angles involving the pyrimidine N atom are also larger in the free tridentate site than in the bound site. The C-N-C and C-C-N angles exhibit trends similar to those described above.

**$^1$H NMR spectra**: Several factors affect the chemical shifts of the bis-tridentate ligand protons upon metal complexation. The first and most obvious one is the change from a *transoid* to a *cisoid* conformation to permit metal chelation. Whereas in the *transoid* form, the nitrogen lone pairs deshield the ligand protons adjacent to the interannular bond, this is not the case in the *cisoid* form. Secondly, the presence of a coordinated metal influences the chemical shifts of ligand protons. In general, the $^1$H chemical shifts for azaheterocycles bound to $Co^{III}$, $Rh^{III}$, $Ru^{II}$ and $Fe^{II}$ exhibit only slight changes, of the order of solvent effects, upon metal complexation.[25] However, the protons *ortho* to the N atom shift upfield because of the magnetic anisotropy of the bound metal ion[25, 26] and the electron density of the metal $t_{2g}$ orbitals.[27]

The local environment of the protons in the complex is also an important consideration. In the complexes, the tpy's are orthogonal to the bis-tridentate ligand (Fig. 9). The protons *ortho*

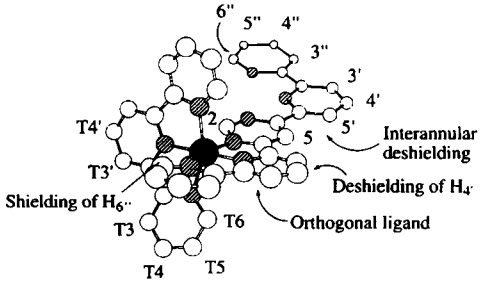


Fig. 9. Shielding and deshielding effects in the bis-tridentate ligands. One $[Ru(tpy)]^{2+}$ moiety has been omitted for clarity.

to the N atom of the terminal pyridines (H T6) are approximately above the shielding zone of the orthogonal ligand pyridine. The protons *para* to the N atom in the central pyridine of the orthogonal ligand (H T4') are held in the deshielding plane of the two terminal pyridine rings. Both these factors have been used as a measure of interligand shielding effects.[28]

In complex **2a**, all of the tpy resonances are slightly shielded relative to $[Ru(tpy)_2]^{2+}$ except for H T4'. The pyrimidine C2 substituent (R) directly affects the chemical shift of H T4', either by allowing the central pyridines of the tpy's to approach one another (R = H), or by not doing so (R = methyl, phenyl and 9-anthryl). The proton resonances of the tpy's in complex **2b** are not greatly influenced by the introduction of the methyl group. All of the protons are shielded relative to $[Ru(tpy)_2]^{2+}$, with H T6 slightly less shielded and H T4' slightly more shielded relative to **2a**. The tpy's in complexes **2c** and **2d**, however, exhibit greater shielding of the protons on the central pyridine due to the phenyl and 9-anthryl substituents, respectively.

The chemical shifts of the bis-tridentate ligands in their complexes are listed in Table 5. Also included is the difference in chemical shift between a given complex and complex **2a** ($\Delta\delta$ **2a**).

Table 5. Chemical shifts and chemical shift differences for complex and ligand protons.

| Cpd. | 6" | 5" | 4" | 3" | 5' | 4' | 3' | 5 | 2 |
|---|---|---|---|---|---|---|---|---|---|
| **3a** | 8.75 | 7.39 | 7.89 | 8.79 | 8.61 | 8.05 | 8.57 | 9.78 | 9.40 |
| **2a** | 7.27 | 7.14 | 7.93 | 8.45 | 9.11 | 8.50 | 8.82 | 9.26 | 6.24 |
| $\Delta\delta$**3a** | −1.48 | −0.25 | +0.04 | −0.34 | +0.50 | +0.45 | +0.25 | −0.52 | −3.24 |
| **2b** | 6.54 | 7.06 [a] | 7.82 [a] | 8.34 [a] | 9.42 | 8.56 | 8.76 | 9.42 | |
| $\Delta\delta$**2a** | −0.73 | −0.08 | −0.11 | −0.11 | +0.31 | +0.06 | −0.06 | +0.16 | |
| **2c** | 5.89 | 7.01 | 7.75 | 8.32 | 9.48 | 8.59 | 8.75 | 9.53 | |
| $\Delta\delta$**2a** | −1.38 | −0.13 | −0.18 | −0.13 | +0.37 | −0.09 | −0.07 | +0.27 | |
| **2d** | 5.49 | 6.80 | 7.64 | 8.24 | 9.80 | 8.64 | 8.74 | 10.02 | |
| $\Delta\delta$**2a** | −1.78 | −0.34 | −0.29 | −0.21 | +0.69 | +0.14 | −0.08 | +0.80 | |

[a] Denotes central position of multiplet; solvents: $CD_3CN$ (complexes), $CDCl_3$ (ligand).

This $\Delta\delta$**2a** value takes into consideration the conformational rearrangement of the ligand that occurs upon metal complexation. The addition of two $[Ru(tpy)]^{2+}$ moieties to ligand **3a** causes proton shifts relative to **2a** similar to those seen in tpy when complexed by ruthenium. The major effects observed are the shielding of H 6" and the deshielding of the H 5', H 4' and H 3' protons, for reasons similar to those previously stated for the ancillary tpy's (Fig. 9). The H 6" proton in the other three dimetallic complexes is increasingly shielded relative to **2a** along with the size of the central substituent. The larger pyrimidine C2 substituents force the tpy's to diverge, moving the shielding zone of the central pyridine of the tpy closer to H 6". The $\Delta\delta$ **2a** values are −0.73 ppm for **2b**, −1.38 ppm for **2c** and −1.78 ppm for **2d**. These values follow the decrease in distance between H 6" and the central pyridine centroid as measured from the X-ray structures (Table 6). This distance is almost identical in **2b** and

Table 6. Relationship between chemical shift and intramolecular distances (see Fig. 9).

| | C6"–Tpy centroid (Å) | $\Delta\delta$ **2a** H 6" (ppm) | C5'–C5 (Å) | $\Delta\delta$ **2a** H 5 (ppm) | $\Delta\delta$ **2a** H 5' (ppm) |
|---|---|---|---|---|---|
| **2a** | 4.292 | 0 | 3.076 | 0 | 0 |
| **2b** | 3.734 | −0.73 | 3.030 | +0.16 | +0.31 |
| **2c** | 3.732 | −1.38 | 3.047 | +0.27 | +0.37 |
| **2d** | 3.640 | −1.78 | 3.022 | +0.80 | +0.69 |

**2c**; the greater shielding of H 6" may be due to the phenyl shielding cone. The remaining protons on the terminal pyridines are also increasingly shielded through the series **2b–d**, albeit to a smaller extent.

Both H 5 and H 5' are increasingly deshielded through the series of dimetallic complexes from **2a** to **2d**. If deshielding were only the result of dinucleation of the pyrimidine, then their chemical shifts would be expected to stay relatively constant throughout the series. On the other hand, the pinching angle of the bis-tridentate ligand should influence the distance from pyrimidine C 5 to the adjacent pyridine C 5'. As this distance diminishes, H 5 and H 5' approach one another and the deshielding increases (Fig. 9). The correlation is not perfect (cf. **2b** and

2c in Table 6), indicating that other factors also influence the chemical shifts of H5 and H5'.

The 9-anthryl group in **3d** can be used as a probe for obtaining information about the solution structure of **2d** (Figs. 10 and 11). The tpy's are strongly shielded because of the 9-anthryl moiety, and NOE interactions exist between them. The HA10 and HA4 protons interact with each other as well as with HT3' from the tpy's. Interestingly, there is no HA10–HT4' interaction; however, an HA4–HT3 interaction indicates that the tpy has moved across the face of the 9-anthryl group and that HA4 and HT3 are close enough to interact. The "rocking" of the tpy back and forth across the two faces of the 9-anthryl group is further corroborated by HA2–HT5, HA2–HT3 and HA2–HT4 interactions. When HA2 interacts with HT3 and HT4 at one extreme of the rocking motion, HA2 on the opposite end of the 9-anthryl moiety interacts with HT5. The symmetry of the $^1$H NMR spectrum indicates that the rocking motion is fast on the NMR timescale.

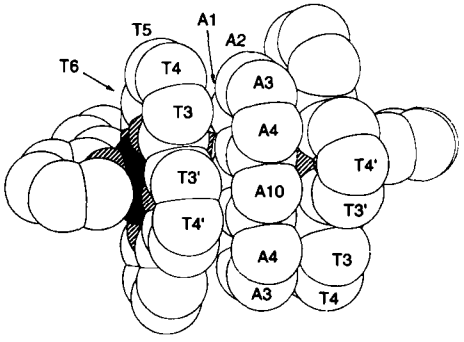


Fig. 10. Labelled space-filling representation of **2d**.

NOE's are also present along the ligand backbone between the protons *ortho* to the interannular bonds. An H4'–H3'' interaction is present, but not an H3'–H4'' one, indicating that the bipyridyl moieties are somewhat distorted. The H4'–H3'' interaction may be caused by the ligand changing shape to alleviate steric repulsion between the 9-anthryl group and the tpy's. No H5–H4' interaction is found, signifying that the ligand distortion is occurring primarily between the two pyridines and not between the pyrimidine and the adjacent pyridine. There are no interactions between the ligand backbone and the tpy's.

**UV/vis spectra**: The UV/vis spectra of the complexes exhibit absorption bands characteristic of Ru$^{II}$ complexes of heterocyclic ligands.[9] The UV region of the absorption spectra is dominated by ligand-centred (LC) $\pi-\pi^*$ bands (Table 7, Fig. 12), which have previously been shown to be roughly additive.[29] The sum of the absorptions due to tpy and the bis-tridentate ligands gives a total of five and six LC bands for the mono- and dimetallic complexes, respectively. Metal coordination to the bis- tridentate ligands leads to numerous LC transitions, as has been found for tpy itself.[30] The low-energy absorption bands for the complexes are caused by either

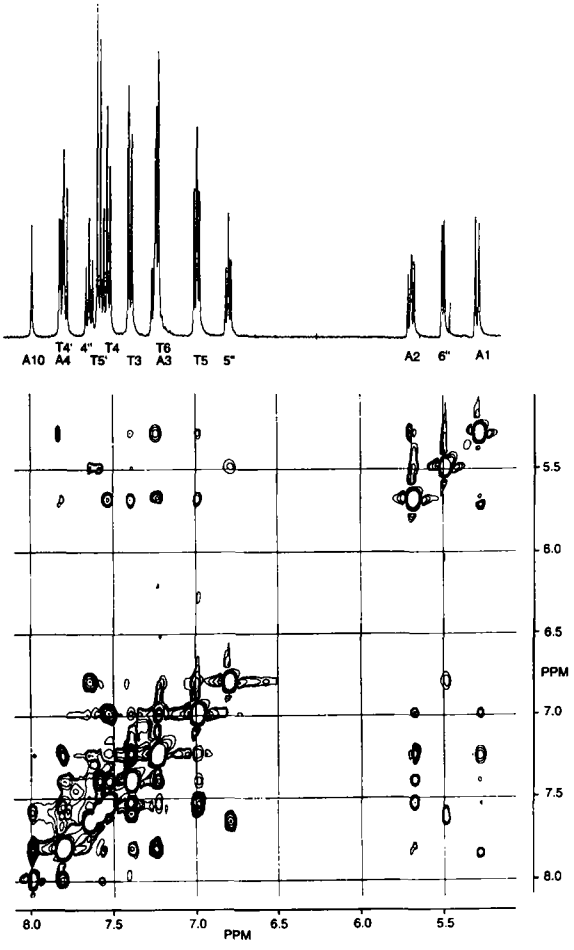


Fig. 11. Proton NMR ROESY spectrum of **2d** at 400 MHz in $CD_3CN$.

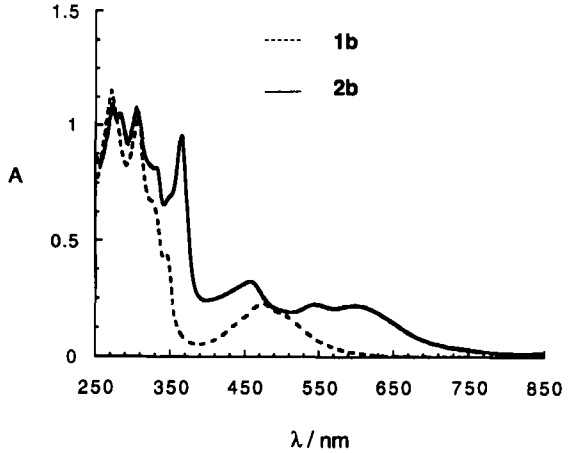


Fig. 12. Electronic absorption spectra of **1b** and **2b**, $10^{-5}$ M in $CH_3CN$.

Table 7. Electronic absorption spectral data for the complexes **1a**–**1c** and **2a**–**2d** in acetonitrile ($\varepsilon$ in $10^4$ M$^{-1}$ cm$^{-1}$).

| Complex | $d_\pi-\pi^*$ (BL) | $d_\pi-\pi^*$ (tpy) | $\pi-\pi^*$ |
|---|---|---|---|
| $[Ru(tpy)(\mathbf{3a})]^{2+}$ (**1a**) | 501 (0.94) | 472 (1.1) | 341 (3.3), 326 (4.2), 308 (5.2), 270 (4.6), 236 (5.0) |
| $[Ru(tpy)(\mathbf{3b})]^{2+}$ (**1b**) | 502 (0.84) | 474 (1.1) | 344 (2.1), 326 (3.1), 307 (4.8), 271 (5.4), 232 (4.1) |
| $[Ru(tpy)(\mathbf{3c})]^{2+}$ (**1c**) | 511 (0.53) | 475 (0.57) | 345 (1.5), 329 (2.0), 310 (2.4), 271 (2.2), 233 (2.7) |
| $[\{Ru(tpy)\}_2(\mathbf{3a})]^{4+}$ (**2a**) | 646 (sh), 616 (1.0), 550 (1.1) | 454 (1.8) | 363 (5.0), 329 (4.9), 302 (6.2), 282 (6.0), 270 (6.3), 226 (6.9) |
| $[\{Ru(tpy)\}_2(\mathbf{3b})]^{4+}$ (**2b**) | 611 (1.4), 550 (1.5) | 456 (2.2) | 365 (6.4), 333 (5.4), 304 (7.2), 283 (7.0), 273 (7.2), 232 (8.6) |
| $[\{Ru(tpy)\}_2(\mathbf{3c})]^{4+}$ (**2c**) | 609 (1.0), 556 (0.93) | 456 (1.5) | 366 (4.0), 333 (3.7), 307 (4.4), 284 (4.7), 274 (4.5), 232 (5.2) |
| $[\{Ru(tpy)\}_2(\mathbf{3d})]^{4+}$ (**2d**) | 617 (1.7), 560 (1.5) | 463 (2.4) | 367 (7.4), 350 (5.2), 329 (5.2), 282 (8.6), 269 (9.2), 230 (12) |



0947-6539/96/0210-1298 $ 15.00+.25/0 Chem. Eur. J. 1996, 2, No. 10

pyrimidine LC absorptions shifted to lower energy owing to metal complexation or to high-energy MLCT absorptions.

The binding of a second metal in the dimetallic complexes **2** results in a red shift of the low-energy absorption with respect to the corresponding monometallic species **1**. The $\pi^*$ levels of the bridging ligand are stabilised by the positive charge on the second ruthenium centre and the associated MLCT bands are observed from $\approx$345 to $\approx$365 nm. An additional absorption band is observed near 282 nm.

The visible absorption spectra are dominated by MLCT bands (Table 7, Fig. 12). The high-energy absorption bands of the monometallic complexes **1** are all near $\lambda_{max}$ = 472 nm. They arise from the $Ru^{II}$-to-tpy MLCT transition. The absorption near 504 nm is ascribed to the $Ru^{II}$-to-bridging-ligand (BL) charge-transfer transition. Similarly, $[Ru(bpy)_2(bpym)]^{2+}$ (bypm = 2,2′-bipyrimidine) is reported to exhibit a high-energy bpy MLCT band at 422 nm, with a lower energy shoulder at 480 nm ascribed to $Ru^{II}$-to-bpym charge transfer.[31, 32]

Several changes occur in the visible spectra on going from the monometallic to the dimetallic complexes: i) the dimetallic complexes exhibit a third MLCT band (near 610 nm); ii) the absorption band near 504 nm undergoes a red shift to 555 nm; and iii) the absorption band near 470 nm exhibits a blue shift to 455 nm. The first two phenomena are probably a result of the splitting and lowering of the bis-tridentate ligand $\pi^*$ level. The complex $[Ru(bpym)_3]^{2+}$ exhibits two low-energy MLCT bands at 418 nm and 454 nm,[31] indicating a splitting in the bpym $\pi^*$ level. A splitting and stabilisation of the bpym $\pi^*$ level was also observed for $[Ru(bpy)_2(bpym)]^{2+}$ ($\lambda_{max}$ = 478 nm) and $[(Ru(bpy)_2)_2(bpym)]^{4+}$ ($\lambda_{max}$ = 545 and 594 nm).[32] These effects are confirmed by the electrochemical results since the bis-tridentate ligands are reduced at less negative potentials in the dimetallic complexes than in the monometallic complexes. The lowest energy bands near 550 and 610 nm are ascribed to the splitting of the $\pi^*$ level of the bridging ligand and subsequent red shift due to the coordination of a second metal. Finally, the increase in the tpy MLCT transition energy is attributed to a stabilisation of the first metal centre on coordination of a second.[29, 32]

**Electrochemistry**: The mono- and dimetallic complexes are stable under the conditions used for the electrochemical studies, and all exhibited well-behaved multiple oxidations and reductions in acetonitrile and DMF solutions. In the positive potential region, the redox processes correspond to metal-localised oxidations. In acetonitrile, a series of ligand-based reductions led to the precipitation and adsorption of the formally neutral complex on the electrode surface. In DMF solutions, the reductions of the complexes were reversible. The cyclic voltammetric values for the mono- and dimetallic complexes are listed in Table 8.

All monometallic complexes **1** exhibited less negative first reduction potentials than the corresponding bis-tridentate ligands **3**.[33] Since pyrimidine is more easily reduced than pyridine,[16] the first reduction of the monometallic complexes was assigned to a pyrimidine-based process. For all monometallic complexes, it was fully reversible, with that of **1b** being at slightly less negative potentials than those of **1a** and **1c**. Further reductions observed at more negative potentials were ascribed to the ancillary tpy groups (Table 8).

The dimetallic complexes **2a–d** exhibited a facile one-electron reduction in the range −0.43 to −0.49 V, which is less negative than the first reduction for the monometallic complexes. Complexation of a second metal centre has previously been shown to facilitate the reduction of the bridging ligand, as may be expected.[29, 32] A second one-electron reduction wave was observed in the range −1.03 to −1.09 V. Both these one-electron processes were attributed to reduction at the pyrimidyl moieties. In addition, the dimetallic complexes exhibited further reductions owing to the ancillary tpy groups that, in acetonitrile solutions, caused the adsorption of the complex on the electrode surface once the complex was formally neutral (four electrons). Reoxidation or further reduction of the complexes then led to the redissolution of the compound, shown by the sharp stripping peaks. In DMF, all reduction processes were reversible. A DMF solution of **3d** exhibited a total of six reversible reductions at −0.35 [60], −0.94 [60], −1.42 [60], −1.55 [60], −1.79 [60] and −2.07 V [60] (Fig. 13, Table 8).

Table 8. Oxidation and reduction potentials for the mono- and dimetallic complexes in acetonitrile [a].

| | $E^{\circ\prime}$ (2) | $E^{\circ\prime}$ (1) | $E^{\circ\prime}$ (1) | $E^{\circ\prime}$ (2) | $E^{\circ\prime}$ (3) | $E^{\circ\prime}$ (4, 5, 6) |
|---|---|---|---|---|---|---|
| **1a** | | +1.33 [80] | −0.90 [60] | −1.47 [d] | −1.34 [c] | |
| **1b** | | +1.45 [60] | −0.88 [40] | −1.34 [c] | −1.30 [b] | −1.42 [c] |
| **1c** | | +1.34 [60] | −0.91 [80] | −1.42 [60] | −1.75 [80] | −2.04 [80] |
| **2a** | +1.57 [60] | +1.41 [60] | −0.43 [60] | −1.03 [60] | −1.45 [b] | −1.47 [c], −1.57 [c] |
| **3a** | | | −1.44 [70] | −2.07 [d] | | |
| **2b** | +1.52 [60] | +1.39 [60] | −0.49 [60] | −1.09 [50] | −1.40 [b] | −1.40 [c], −1.57 [c] |
| **3b** | | | −1.49 [60] | −2.17 [d] | | |
| **2c** | +1.53 [60] | +1.40 [60] | −0.47 [60] | −1.05 [50] | −1.51 [b] | −1.53 [c], −1.63 [c] |
| **3c** | | | −1.43 [60] | −2.06 [d] | | |
| **2d** | +1.58 [60] | +1.41 [60] | −0.45 [60] | −1.07 [50] | −1.42 [b] | −1.52 [c], −1.58 [c] |
| **3d** | | | −1.46 [70] | −1.96 [d] | −2.06 [d] | |

[a] vs. SCE. [b] Stripping peak. [c] Adsorption peak. [d] Irreversible process.

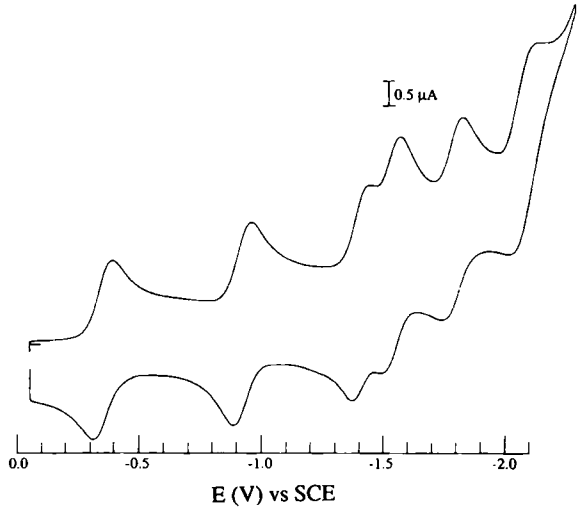


Fig. 13. Cyclic voltammogram of the ligand-based reductions of **2d** in DMF.

In the positive potential region, metal-based oxidations were observed for all of the complexes. The monometallic complexes displayed one-electron oxidations at slightly more positive potentials than $[Ru(tpy)_2]^{2+}$ (+1.29 V),[34] indicating that the bis-tridentate ligands **3a–d** are stronger electron acceptors than tpy. The oxidation potential of **1b** was more positive than the other two monometallic complexes. The dimetallic complexes exhibited two distinct waves corresponding to each $Ru^{II}/Ru^{III}$ oxidation (Fig. 14, Table 8).

The degree of metal–metal interaction in dimetallic complexes was previously estimated by examination of i) the differences in the first reduction potential of bridging ligand in the mono- and dimetallic complexes ($\Delta E^{\circ\prime}_{red1Ru2} - \Delta E^{\circ\prime}_{red1Ru}$); ii) spectral

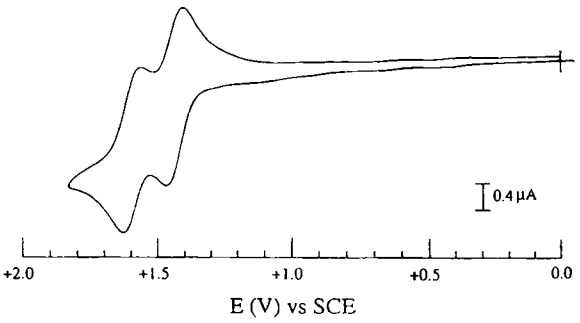


Fig. 14. Cyclic voltammogram of the metal-based oxidation of **2a** in acetonitrile.

shifts in MLCT bands between mono- and dimetallic complexes ($\Delta\lambda_{BLRu2} - \Delta\lambda_{BLRu}$); iii) differences in the metal first oxidation potential between mono- and oligonuclear complexes ($\Delta E^{o\prime}_{ox1Ru2} - \Delta E^{o\prime}_{ox1Ru}$); iv) differences between the metal first and second oxidation potentials in the dimetallic complexes ($\Delta E^{o\prime}_{ox2Ru2} - \Delta E^{o\prime}_{ox1Ru2}$).[29] The comproportionation constants ($K_c$) for the dimetallic complexes were calculated (at $T = 298$ K) for the equilibrium (1) and the corresponding equation (2).[35]

$$Ru^{II}-Ru^{II} + Ru^{III}-Ru^{III} \rightleftharpoons 2\,Ru^{II}-Ru^{III} \quad (1)$$

$$K_c = \exp\left(\frac{\Delta E(mv)}{25.69}\right) \quad (2)$$

The mono- and dimetallic complexes of the bis-tridentate ligands exhibit metal–metal interactions based on the above criteria (Table 9). The splitting of the bis-tridentate ligand LUMO

Table 9. Evaluation of the criteria for metal–metal communication [a].

| Mono- and dimetallic complexes [b] | Criterion (i) $\Delta E^{o\prime}_{red1Ru2} - \Delta E^{o\prime}_{red1Ru}$ | Criterion (ii) $\Delta\lambda_{BLRu2} - \Delta\lambda_{BLRu}$ [d] | Criterion (iii) $\Delta E^{o\prime}_{oxRu2} - \Delta E^{o\prime}_{oxRu}$ | Criterion (iv) $\Delta E^{o\prime}_{ox2Ru2} - \Delta E^{o\prime}_{ox1Ru2}$ | $K_c$ |
|---|---|---|---|---|---|
| Ru **3a**–$Ru_2$ **3a** | +0.47 V | +115 | +0.07 V | +0.16 V | $5.1 \times 10^2$ |
| Ru **3b**–$Ru_2$ **3b** | +0.39 V | +109 | −0.06 V | +0.13 V | $1.6 \times 10^2$ |
| Ru **3c**–$Ru_2$ **3c** | +0.44 V | +106 | +0.07 V | +0.13 V | $1.6 \times 10^2$ |
| $Ru_2$**3d** [c] | | | | +0.17 V | $7.5 \times 10^2$ |

[a] See text. [b] Terpyridine as ancillary ligand. [c] Monometallic complex not isolated. [d] 49 nm.

made the interpretation of the bridging-ligand MLCT spectral changes difficult. The net effect in the dimetallic complexes is a red shift of the bis-tridentate ligand MLCT bands. It was shown that the pyrimidine (L) bridged $[\{Ru(bpy)_2(Cl)\}_2(L)]^{4+}$ dimetallic complexes experienced a blue shift of the pyrimidine MLCT absorption band compared with the monometallic complex. With L = pyrazine, the pyrazine MLCT absorption band was red-shifted compared with the monometallic complex.[36]

The variation in the first oxidation potential for the **1b**–**2b** pair (− 0.10 V) did not show an increase for the dimetallic complex, as one would expect, whereas the **1a**–**2a** and **1c**–**2c** pairs did. The $\Delta E^{o\prime}$ separation between two metal-based oxidation potentials and the comproportionation constants were previously utilised as direct experimental parameters for examining metal–metal interactions.[35] From these parameters, we see that the dimetallic complexes **2a** – **2d** exhibit moderate metal–metal interaction.

## Conclusion

The series of mono- and dimetallic complexes of rack-like [1]R and [2]R described in the present work represent the first and simplest members of this class of substances. The crystal structure data, revealing shape and geometrical features, provide information about the structural requirements for extension of this type of coordination array towards higher nuclearity. In particular, the central substituents allow the control of the overall shape of the unit. Thus, a methyl group leads to a straightening of the structure and so appears to provide geometrical properties best suited for rack, ladder and grid formation. A slightly less bulky substituent (e.g., a carboxyl group) could result in parallel ancillary ligands.

The electrochemical data indicate the functional properties that extended racks may possess: interaction between the metal centres and along the rack backbone, so that such species represent frameworks along which redox-regulated communication between active centres may occur. Mixed-metal racks are also being considered. The mixed-valence and luminescence properties of these complexes will be the subject of another publication. The synthesis of longer rack complexes, as well as ladders and grids, is currently being pursued. Such species represent potential components for the design of molecular and supramolecular electronic devices.[1b]

## Experimental Procedure

**Materials**: Reagent solutions were added against an Ar counterstream and bubbled with Ar for 15 min. Solvents were removed with a rotary evaporator at water aspirator pressure. Precipitates were isolated by high-speed spinning in a Hettich Universal centrifuge (≈3000 rpm, 5 min). Chromatography was carried out on Merck act. II–III alumina (0.063–0.200 mm). Reactions and chromatography fractions were analysed with Macherey–Nagel Polygram Alox N/$UV_{254}$ alumina plates. Unless otherwise noted, $^1$H NMR spectra were measured in $CD_3CN$ calibrated to the residual solvent peak at 200 MHz on a Bruker AC200 spectrometer. Melting points were obtained with a digital Thomas Hoover (Electrotherma) apparatus. Infrared absorption spectra were recorded on a Perkin Elmer 1600 series FTIR spectrometer in KBr, and electronic absorption spectra on a Cary 219 spectrometer in $CH_3CN$, with $\lambda_{max}$ in nm and $\varepsilon$ ($\times 10^4$) in $M^{-1}cm^{-1}$. Fast atom bombardment (FAB) mass spectroscopy was performed on a ZAB-HF VG spectrometer with *m*-nitrobenzyl alcohol as the matrix. Cyclic voltammograms were measured on a EDT potentionstat/galvanostat with a Tacussel IG5-LN integrator and IFELEC-IF 3802 recorder: the working electrode was a platinum disc, the auxillary electrode a coiled platinum wire and the reference electrode an SCE. Tetra-*n*-butylammonium hexafluorophosphate (TBAH), recrystallised three times from ethyl acetate, was used as the supporting electrolyte. The solutions were deaerated with Ar and measurements were made under an Ar atmosphere. Spectroscopic studies were performed in spectroscopic-grade acetonitrile. All solvents were reagent grade and used without further purification. Ru(tpy)$Cl_3$ [37], 2,2′:6′,2″-terpyridine [33] and ligands **3a**–**d** [33] were prepared as described elsewhere.

**Crystal structure determinations**: Diffraction experiments were performed on a STOE IPDS diffractometer with $Mo_{K\alpha}$ radiation ($\lambda = 0.71069$ Å) with empirical absorption corrections. Machine parameters, crystal data and data collection parameters are summarised in Table 10 [38]. The data were processed with SHELXS-86, SHELXL-93 and SCHAKAL92. Refinements were carried out with full-matrix least-squares techniques on $F^2$. H atoms were refined isotropically and all other atoms were refined anisotropically.

Green crystals of the dimetallic complexes suitable for X-ray diffraction were grown by slow diffusion of diethylether into acetonitrile or acetone solutions. Crystals of **2a** formed as the trisacetone solvate of the complex ($C_{64}H_{56}F_{24}N_{12}O_3P_4Ru_2$) with $M = 1811.22$. The trisacetonitrile solvate of **2b** ($C_{61}H_{49}F_{24}N_{15}P_4Ru_2$) with $M = 1774.17$ crystallised from acetonitrile/ether. The bis-acetonitrile solvate of **2c** ($C_{64}H_{48}F_{24}N_{14}P_4Ru_2$) with $M = 1795.18$ crystallised from a similar solvent system. Crystals of **2d** formed as the acetone solvate of the complex ($C_{71}H_{52}F_{24}N_{12}OP_4Ru_2$), $M = 1871.33$, by ether diffusion into an acetonitrile/acetone mixture of the complex. Red crystals of **1c**, $C_{48}H_{37}F_{12}N_9OP_2Ru$, with $M = 1146.88$, crystallised from acetone/ether.

**[Ru(tpy)(3a)][$PF_6$]$_2$ (1a)** and **[{Ru(tpy)}$_2$(3a)][$PF_6$]$_4$ (2a)**: To Ru(tpy)$Cl_3$ (0.0391 g, 0.888 mmol) and **3a** (0.0138 g, 0.355 mmol) was added ethanol/water (10 mL, 1:1), and the mixture was heated at reflux for 22 h, cooled to room temperature and



0947-6539/96/0210-1300 $ 15.00+.25/0 Chem. Eur. J. 1996, 2, No. 10

Table 10. Crystal and data collection parameters for complexes **1c** and **2a–d**.

| | **1c** | **2a** | **2b** | **2c** | **2d** |
|---|---|---|---|---|---|
| formula weight | 1146.88 | 1811.22 | 1774.17 | 1795.18 | 1871.33 |
| space group | $P2(1)/n$ (no. 14) | $Pnma$ (no. 62) | $P\bar{1}$ (no. 2) | $P\bar{1}$ (no. 2) | $P\bar{1}$ (no. 2) |
| crystal system | monoclinic | orthorhombic | triclinic | triclinic | triclinic |
| $a$, Å | 14.519(6) | 15.751(4) | 13.354(3) | 13.196(4) | 12.446(5) |
| $b$, Å | 15.515(5) | 25.110(14) | 15.007(2) | 15.079(4) | 13.236(5) |
| $c$, Å | 21.774(6) | 17.797(9) | 18.824(3) | 18.618(6) | 23.046(8) |
| $\alpha$, ° | 90 | 90 | 75.67(2) | 74.34(2) | 102.25(2) |
| $\beta$, ° | 98.93(2) | 90 | 72.23(2) | 75.58(2) | 97.87(2) |
| $\gamma$, ° | 90 | 90 | 75.00(2) | 75.74(2) | 102.30(2) |
| $V$, Å$^3$ | 4845(3) | 7039(6) | 3411.3(10) | 3390(2) | 3558(2) |
| $\rho_{calc}$, g cm$^{-3}$ | 1.572 | 1.709 | 1.727 | 1.758 | 1.747 |
| $Z$ | 4 | 4 | 2 | 2 | 2 |
| $\mu$, mm$^{-1}$ | 0.484 | 0.639 | 0.656 | 0.660 | 0.600 |
| $\lambda$, Å | 0.71069 | 0.71069 | 0.71069 | 0.71069 | 0.71069 |
| $T$, K | 200(2) | 200(2) | 200(1) | 200(1) | 203(2) |
| $2\theta_{max}$, ° | 56 | 56 | 56 | 54 | 56 |
| total reflns | 38634 | 39284 | 36042 | 19837 | 38111 |
| unique reflns | 11619 | 8621 | 14975 | 12635 | 15730 |
| data/restraints | 11585 / 0 | 8618 / 0 | 14965 / 0 | 12600 / 0 | 15728 / 0 |
| parameters refined | 707 | 496 | 958 | 975 | 1186 |
| $R_1$, % [$I > 2\sigma(I)$] | 7.89 | 8.40 | 7.18 | 6.32 | 6.89 |

filtered. An excess of aqueous $[NH_4][PF_6]$ was added to the filtrate and the resulting precipitate was collected. The solid was purified by successive recrystallisations from acetonitrile/toluene to afford **2a** (0.0421 g, 72%) as a green solid. The recrystallisation filtrates were combined, the solvent was removed and the crude product was chromatographed on alumina with acetonitrile/toluene (1:1) to afford **1a** (0.0045 g, 13%) as a red solid.

**1a**: $^1$H NMR: peaks integrating to 27 H; FAB MS: $m/z$ (%) = 868 (82) [$M$ − 145 (− $PF_6$)], 723 (100) [$M$ − 290 (− 2$PF_6$)], 489 (50) [$M$ − 333 (− 2$PF_6$, −tpy)]; Anal. calcd. for $C_{39}H_{27}F_{12}N_9P_2Ru \cdot 2(CH_3)_2CO$: C 47.88, H 3.48, N 11.17, found: C 47.07, H 3.28, N 10.45; IR (KBr): $\tilde{\nu}$ = 1601, 1447, 1082, 842, 558 cm$^{-1}$; UV/vis: $\lambda$ = 236 (5.0), 270 (4.6), 308 (5.2), 326 (4.2), 341 (3.3), 472 (1.1), 501 (0.94) nm.

**2a**: M.p.: >300 °C; $^1$H NMR: $\delta$ = 9.26 (d, H5, $J$ = 1.1 Hz, 1H), 9.11 (dd, H5′, $J$ = 8.2, 0.7 Hz, 2H), 8.82 (dd, H3′, $J$ = 8.1, 0.7 Hz, 2H), 8.67 (d, HT3′, $J$ = 8.2 Hz, 4H), 8.50 (dd, H4′, $J$ = 8.4, 7.8 Hz, 2H), 8.50 (t, HT4′, $J$ = 8.2 Hz, 6H), 8.45 (d, H3″, $J$ = 7.8 Hz, 2H), 8.36 (dt, HT3, $J$ = 7.3, 1.4 Hz, 4H), 7.93 (td, H4″, $J$ = 7.8, 1.5 Hz, 2H), 7.82 (td, HT4, $J$ = 7.9, 1.5 Hz, 4H), 7.27 (d, H6″, $J$ = 5.1 Hz, 2H), 7.14 (ddd, H5″, $J$ = 6.7, 5.5, 1.1 Hz, 2H), 7.05 (d, HT6, $J$ = 5.4 Hz, 4H), 6.96 (ddd, HT5, $J$ = 7.3, 5.5, 1.1 Hz, 4H), 6.24 (d, H2, $J$ = 0.7 Hz, 1H); FAB MS: $m/z$ (%) = 1491 (10) [$M$ − 144 (− $PF_6$)], 1347 (30) [$M$ − 288 (− 2$PF_6$)], 1202 (20) [$M$ − 333 (− 3$PF_6$]; Anal. calcd. for $C_{54}H_{38}F_{24}N_{12}P_4Ru_2$: C 39.61, H 2.34, N 10.27, found: C 38.50, H 2.62, N 10.88; IR (KBr): $\tilde{\nu}$ = 1602, 1443, 1384, 843, 772, 557 cm$^{-1}$; UV/vis: $\lambda$ = 226 (6.9), 271 (6.3), 282 (6.0), 302 (6.2), 329 (4.9), 363 (5.0), 454 (1.8), 550 (1.1), 616 (1.0), 646 sh nm.

**[{Ru(tpy)}$_2$(3b)][PF$_6$]$_4$ (2b)** and **[Ru(tpy)(3b)][PF$_6$]$_2$ (1b)**: Compounds **1b** (0.0066 g, 8.2%) and **2b** (0.0651 g, 49%) were prepared from **3b** (0.0324 g, 0.0806 mmol) and $Ru(tpy)Cl_3$ (0.0774 g, 0.176 mmol) following the same procedure as for **1a** and **2a**.

**1b**: $^1$H NMR: peaks integrating to 29 H; MS FAB: $m/z$ (%) = 882 (5) [$M$ − 144 (− $PF_6$)], 736 (50) [$M$ − 290 (− 2$PF_6$)], 503 (35) [$M$ − 523 (− 2$PF_6$, −tpy)]; Anal. calcd. for $C_{40}H_{29}F_{12}N_9P_2Ru \cdot (CH_3)_2CO$: C 47.55, H 3.25, N 11.61; found: C 47.23, H 3.14, N 11.28; IR (KBr): $\tilde{\nu}$ = 1602, 1448, 1386, 1284, 842, 770, 558 cm$^{-1}$; UV/vis: $\lambda$ = 232 (4.1), 271 (5.4), 307 (4.8), 326 (3.1), 344 (2.1), 474 (1.1), 502 (0.84) nm.

**2b**: M.p.: >300 °C; $^1$H NMR: $\delta$ = 9.42 (s, H5, 1H), 9.42 (d, H5′, $J$ = 8.4 Hz, 2H), 8.76 (d, H3′, $J$ = 8.1 Hz, 2H), 8.63 (d, HT3′, $J$ = 8.4 Hz, 4H), 8.56 (t, H4′, $J$ = 8.0 Hz, 2H), 8.39 (d, H3″, $J$ = 7.6 Hz, 2H), 8.35 (t, HT4′, $J$ = 8.8 Hz, 2H), 8.32 (d, HT3, $J$ = 8.0 Hz, 4H), 7.81 (m, H4″, T4, 6H), 7.18 (d, HT6, $J$ = 5.5 Hz, 4H), 7.14 – 6.99 (m, H5″, T5, 6H), 6.54 (d, H6″, $J$ = 5.1 Hz, 2H), 1.02 (s, HMe, 3H); ($CD_3COCD_3$): $\delta$ = 9.90 (s, H5, 1H), 9.56 (d, H3′ or 5′, $J$ = 8.4 Hz, 2H), 9.09 (d, H3′, $J$ = 8.1 Hz, 2H), 8.93 (d, HT3′, $J$ = 8.2 Hz, 4H), 8.71 (dt, H3″, $J$ = 8.0, 1.8 Hz, 2H), 8.67 (t, HT4′ or 4′, $J$ = 8.1 Hz, 2H), 8.62 (dt, HT3, $J$ = 8.0, 0.7 Hz, 4H), 8.52 (t, HT4′ or 4′, $J$ = 8.0 Hz, 2H), 8.01 (td, HT4, $J$ = 8.1, 1.5 Hz, 4H), 7.97 (td, H4″, $J$ = 6.6, 1.5 Hz, 2H), 7.46 (d, HT6, $J$ = 5.1 Hz, 4H), 7.27 (ddd, H5″, $J$ = 7.7, 5.8, 1.1 Hz, 2H), 7.16 (ddd, HT5, $J$ = 7.7, 5.5, 1.1 Hz, 4H), 7.02 (d, H6″, $J$ = 4.8 Hz, 2H), 1.34 (s, HMe, 3H); FAB MS: $m/z$ (%) = 1506 (63) [$M$ − 143 (− $PF_6$], 1361 (100) [$M$ − 289 (− 2$PF_6$)], 1216 (37) [$M$ − 434 (− 3$PF_6$)], 1060 (20) [$M$ − 582 (− 4$PF_6$)]; Anal. calcd. for $C_{55}H_{40}F_{24}N_{12}P_4Ru_2 \cdot 2(CH_3)_2CO$: C 41.40, H 2.96, N 9.50; found: C 40.87, H 3.21, N 9.06; IR (KBr): $\tilde{\nu}$ = 1603, 1452, 1384, 848, 773, 558 cm$^{-1}$; UV/vis: $\lambda$ = 232 (8.6), 273 (7.2), 283 (7.0), 304 (7.2), 333 (5.4), 365 (6.4), 456 (2.2), 550 (1.5), 611 (1.4) nm.

**[{Ru(tpy)}$_2$(3c)][PF$_6$]$_4$ (2c)** and **[Ru(tpy)(3c)][PF$_6$]$_2$ (1c)**: Compounds **1c** (0.0117 g, 7.6%) and **2c** (0.1371 g, 56%) were prepared from **3c** (0.0660 g, 0.142 mmol) and $Ru(tpy)Cl_3$ (0.1432 g, 0.3245 mmol) following the same procedure as for **2a** and **1a**.

**1c**: $^1$H NMR: peaks integrating to 31 H; FAB MS: $m/z$ (%) = 944.0 (60) [$M$ − 144 (− $PF_6$)], 814.1 (30) [$M$ − 190 (− 2$PF_6$ + O], 799.1 (100) [$M$ − 289 (− 2$PF_6$)], 564.1 (40) [$M$ − 524 (− 2$PF_6$, −tpy)]; Anal. calcd. for $C_{45}H_{31}F_{12}N_9P_2Ru \cdot 3CH_3CN$: C 50.49, H 3.33, N 13.86; found: C 50.97, H 3.37, N 13.30; IR (KBr): $\tilde{\nu}$ = 1602, 1384, 842, 770, 558 cm$^{-1}$; UV/vis: $\lambda$ = 233 (2.7), 271 (2.2), 310 (2.4), 329 (2.0), 345 (1.5), 475 (0.57), 511 (0.53) nm.

**2c**: M.p.: >300 °C; $^1$H NMR: $\delta$ = 9.53 (s, H5, 1H), 9.48 (d, H5′, $J$ = 8.0, 2H), 8.75 (d, H3′, $J$ = 7.7 Hz, 2H), 8.59 (t, H4′, $J$ = 8.0 Hz, 2H), 8.32 (d, H3″, $J$ = 8.2 Hz, 2H), 8.20–8.04 (m, HT3, T5, m, 10H), 7.80 (td, HT4, $J$ = 7.9, 1.5 Hz, 4H), 7.75 (td, H4″, $J$ = 8.3, 1.7 Hz, 2H), 7.23 (d, HT6, $J$ = 4.9 Hz, 4H), 7.04 (ddd, HT5, $J$ = 7.4, 5.7, 1.2 Hz, 4H), 7.01 (ddd, H5″, $J$ = 7.6, 6.1, 1.5 Hz, 2H), 6.78 (t, $H_p$, $J$ = 7.3 Hz, 1H), 6.35 (d, HT4′, $J$ = 7.7 Hz, 2H), 5.89 (d, H6″, $J$ = 5.6 Hz, 2H), 4.94 (m, $H_o$, 2H); FAB MS: $m/z$ (%) = 1569 (30) [$M$ − 143 (− $PF_6$)], 1424 (55) [$M$ − 288 (− 2$PF_6$)], 1278 (20) [$M$ − 334 (− 3$PF_6$)], 1132 (10) [$M$ − 479 (− 4$PF_6$)]; Anal. calcd. for $C_{60}H_{42}F_{24}N_{12}P_4Ru_2 \cdot 3(CH_3)_2CO$: C 43.85, H 3.20, N 8.90; found: C 44.30, H 2.88, N 8.82; IR (KBr): $\tilde{\nu}$ = 1604, 1451, 1384, 1094, 843, 768, 558 cm$^{-1}$; UV/vis: $\lambda$ = 232 (5.2), 274 (4.5), 284 (4.7), 307 (4.4), 333 (3.7), 366 (4.0), 456 (1.5), 556 (0.93), 609 (1.0) nm.

**[{Ru(tpy)}$_2$(3d)][PF$_6$]$_4$ (2d)**: To $Ru(tpy)Cl_3$ (0.0270 g, 0.0613 mmol) and **3d** (0.0140 g, 0.0248 mmol) was added ethylene glycol (40 mL) and *N*-ethylmorpholine (0.3 mL); the mixture was heated under reflux for 20 h, cooled to room temperature and filtered. An excess of aqueous $[NH_4][PF_6]$ was added to the solution and the precipitate was collected. The solid was purified by successive recrystallisations from acetonitrile/toluene to afford **2d** (0.0229 g, 51%) as a green solid. Only a small amount of a red solid, **1d**, was isolated, and was not further characterised.

**2d**: M.p.: >300 °C; $^1$H NMR (400 MHz): $\delta$ = 10.02 (s, H5, 1H), 9.80 (d, H5′, $J$ = 7.8 Hz, 2H), 8.74 (d, H3′, $J$ = 7.6 Hz, 2H), 8.64 (t, H4′, $J$ = 8.0 Hz, 2H), 8.24 (d, H3″, $J$ = 7.9 Hz, 2H), 7.99 (s, HA10, 1H), 7.84–7.76 (m, HA4, T4′, 4H), 7.64 (td, H4″, $J$ = 7.8, 1.3 Hz, 2H), 7.58 (d, HT5′, $J$ = 8.0 Hz, 4H), 7.54 (td, HT4, $J$ = 7.8, 1.4 Hz, 4H), 7.39 (d, HT3, $J$ = 8.1 Hz, 4H), 7.28–7.21 (m, HT6,3, 6H), 6.99 (ddd, HT5, $J$ = 7.5, 5.4, 1.4 Hz, 4H), 6.80 (ddd, H5″, $J$ = 7.5, 5.8, 1.4 Hz, 2H), 5.68 (dd, HA2, $J$ = 8.8, 1.0 Hz, 2H), 5.49 (d, H6″, $J$ = 5.9 Hz, 2H), 5.28 (d, HA1, $J$ = 8.8 Hz, 2H); ES-MS: $m/z$ (%) = 762.0 [$M/2$ (− 2$PF_6$)], 459.6 [$M/3$ (− 3$PF_6$)], 307.8 [$M/4$ (− 4$PF_6$)]; Anal. calcd. for $C_{68}H_{46}F_{24}N_{12}P_4Ru_2 \cdot 3(CH_3)_2CO$: C 46.54, H 3.25, N 8.46; found: C 46.09, H 3.76, N 7.89; IR: $\tilde{\nu}$ = 1604, 1450, 1384, 841, 763, 558 cm$^{-1}$; UV/vis: $\lambda$ = 230 (12), 269 (9.2), 282 (8.6), 329 (5.2), 350 (5.2), 367 (7.4), 463 (2.4), 560 (1.5), 617 (1.7) nm.

**Acknowledgments**: G. S. H. thanks NSERC (Canada) for a doctoral fellowship; C. R. A. is grateful to the Jubiläum Stiftung and for Chateaubriand and NSF-NATO Postdoctoral Fellowships. We thank Patrick Maltese for measuring ROESY spectra.

Received: March 22, 1996 [F327]

[1] a) J.-M. Lehn, *Supramolecular Chemistry*, VCH, Weinheim, **1995**; b) *ibid.*, Ch. 8.
[2] G. S. Hanan, C. R. Arana, J.-M. Lehn, D. Fenske, *Angew. Chem. Int. Ed. Engl.* **1995**, *34*, 1122.
[3] P. Baxter, J.-M. Lehn, J. Fischer, M.-T. Youinou, *Angew. Chem. Int. Ed. Engl.* **1994**, *33*, 2284.
[4] J.-M. Lehn, *Angew. Chem. Int. Ed. Engl.* **1988**, *27*, 89.
[5] V. Balzani, F. Scandola, *Supramolecular Photochemistry*, Ellis Horwood, Chichester, **1991**.
[6] F. A. Cotton, G. Wilkinson, *Advanced Inorganic Chemistry*, 5th ed., Wiley, Toronto, **1988**.
[7] W. R. McWhinnie, J. D. Miller, *Adv. Inorg. Chem. Radiochem.* **1969**, *12*, 135.
[8] E. C. Constable, *Adv. Inorg. Chem. Radiochem.* **1986**, *30*, 69.
[9] A. Juris, V. Balzani, F. Barigelletti, S. Campagna, P. Belser, A. von Zelewsky, *Coord. Chem.* **1988**, *84*, 85.
[10] M.-T. Youinou, N. Rahmouni, J. Fischer, J. A. Osborn, *Angew. Chem. Int. Ed. Engl.* **1992**, *31*, 733.
[11] G. S. Hanan, C. R. Arana, D. Bassani, J.-M. Lehn, unpublished results.
[12] G. S. Hanan, D. Volkmer, J.-M. Lehn, unpublished results.
[13] E. C. Constable, in *Prog. Inorg. Chem.* (Ed.: K. D. Karlin), Wiley, New York, **1994**, *42*, 67.
[14] P. J. Steel, *Coord. Chem. Rev.* **1990**, *106*, 227.
[15] P. Ford, D. F. P. Rudd, R. Gaunder, H. Taube, *J. Am. Chem. Soc.* **1968**, *90*, 1187.
[16] S. D. Ernst, W. Kaim, *Inorg. Chem.* **1989**, *28*, 1520.
[17] *Photochemistry of Polypyridine and Porphyrin Complexes* (Ed.: K. Kalyanasundaram), Academic Press, Suffolk, **1992**.
[18] M. Coruzzi, G. D. Andreetti, V. Bocchi, A. Pochini, R. Ungaro, *J. Chem. Soc. Perkin Trans. II* **1982**, 1133.
[19] R. Ungaro, A. Pochini, G. D. Andreetti, V. Sangermano, *J. Chem. Soc. Perkin Trans. II* **1984**, 1979.

[20] S. C. Rasmussen, S. E. Ronco, D. A. Mlsna, M. A. Billadeau, W. T. Pennington, J. W. Kolis, J. D. Petersen, *Inorg. Chem.* **1995**, *34*, 821.
[21] A. K. Kabi Satpathy, Ph.D. Thesis, Clemson University, **1989**.
[22] C. A. Hunter, J. K. M. Sanders, *J. Am. Chem. Soc.* **1990**, *112*, 5525.
[23] C. A. Bessel, R. F. See, D. L. Jameson, M. R. Churchill, K. L. Takeuchi, *J. Chem. Soc. Dalton Trans.* **1992**, 3223.
[24] G. S. Hanan, J.-M. Lehn, N. Kyritsakas, J. Fischer, *J. Chem. Soc. Chem. Commun.* **1995**, 765.
[25] D. K. Lavallee, M. D. Baughman, M. P. Phillips, *J. Am. Chem. Soc.* **1977**, *99*, 718.
[26] D. K. Lavallee, E. B. Fleischer, *J. Am. Chem. Soc.* **1972**, *94*, 2583.
[27] H. Elsbernd, J. K. Beattie, *J. Inorg. Nucl. Chem.* **1972**, *34*, 771.
[28] R. P. Thummel, Y. Jahng, *Inorg. Chem.* **1986**, *25*, 2527.
[29] G. Denti, S. Campagna, L. Sabatino, S. Serroni, M. Ciano, V. Balzani, *Inorg. Chem.* **1990**, *29*, 4750.
[30] K. Nakamoto, *J. Phys. Chem.* **1960**, *64*, 1420.
[31] D. P. Rillema, G. Allen, T. J. Meyer, D. Conrad, *Inorg. Chem.* **1983**, *22*, 1617.
[32] R. Sahai, L. Morgan, D. P. Rillema, *Inorg. Chem.* **1988**, *27*, 3495.
[33] G. S. Hanan, U. Schubert, D. Volkmer, E. Rivière, J.-M. Lehn, N. Kyritsakas, J. Fischer, unpublished results.
[34] R. C. Young, J. K. Nagle, T. J. Meyer, D. G. Whitten, *J. Am. Chem. Soc.* **1978**, *100*, 4773.
[35] G. Giuffrida, S. Campagna, *Coord. Chem. Rev.* **1994**, *135/136*, 517.
[36] M. J. Powers, T. J. Meyer, *Inorg. Chem.* **1978**, *17*, 2955.
[37] B. P. Sullivan, J. M. Calvert, T. J. Meyer, *Inorg. Chem.* **1980**, *19*, 1404.
[38] Crystallographic data (excluding structure factors) for the structures reported in this paper have been deposited with the Cambridge Crystallographic Data Centre as supplementary publication no. CCDC-1220-25. Copies of the data can be obtained free of charge on application to the Director, CCDC, 12 Union Road, Cambridge CB21EZ, UK (Fax: Int. code +(1223)336-033; e-mail: teched@chemcrys.cam.ac.uk).



0947-6539/96/0210-1302 $ 15.00+.25/0